

# **Bioinspired Zwitterionic Nanowires with Simultaneous Biofouling Reduction and Release**

Jing Wang, Brian Macdonald, Tae H. Cho, Taylor Repetto, Kai Sun, Anish Tuteja,\* and Neil P. Dasgupta\*

Marine biofouling is a complex and dynamic process that significantly increases the carbon emissions from the maritime industry by increasing drag losses. However, there are no existing non-toxic marine paints that can achieve both effective fouling reduction and efficient fouling release. Inspired by antifouling strategies in nature, herein, a superoleophobic zwitterionic nanowire coating with a nanostructured hydration layer is introduced, which exhibits simultaneous fouling reduction and release performance. The zwitterionic nanowires demonstrate >25% improvement in fouling reduction compared to state-of-the-art antifouling nanostructures, and four times higher fouling-release compared to conventional zwitterionic coatings. Fouling release is successfully achieved under a wall shear force that is four orders of magnitude lower than regular water jet cleaning. The mechanism of this simultaneous fouling reduction and release behavior is explored, and it is found that a combination of 1) a mechanical biocidal effect from the nanowire geometry, and 2) low interfacial adhesion resulting from the nanostructured hydration layer, are the major contributing factors. These findings provide insights into the design of nanostructured coatings with simultaneous fouling reduction and release. The newly established synthesis procedure for the zwitterionic nanowires opens new pathways for implementation as antifouling coatings in the maritime industry and biomedical devices.

#### 1. Introduction

Marine biofouling has remained a persistent problem throughout human history.[1] It not only inhibits deep-ocean exploration and costs billions of dollars per year,[1b] but also increases the greenhouse gas emission from ships by at least 20%, which represents ≈80% of global trade by volume.[2] Marine fouling is a complex and dynamic process, where various species accrete, compete, and cooperate during their attachment to the exposed surfaces, forming living and developing biofilms with a variety of multi-scale adhesion mechanisms.[1] Biofilms can disrupt the performance of antifouling coatings by changing their surface chemistry and burying their surface micro/nano structures,[3] adhering strongly to their surfaces, and further dynamically adapting to shear flow environments.[1a,4] In particular, it is challenging to simultaneously achieve both a large reduction in the rate of marine fouling and easy removal of the accumulated biofilms using a single antifouling coating.

J. Wang<sup>[+]</sup>, T. H. Cho, N. P. Dasgupta Department of Mechanical Engineering University of Michigan Ann Arbor, MI 48109, USA E-mail: ndasgupt@umich.edu

B. Macdonald, T. Repetto, A. Tuteja, N. P. Dasgupta Department of Materials Science and Engineering

University of Michigan Ann Arbor, MI 48109, USA E-mail: atuteja@umich.edu



The ORCID identification number(s) for the author(s) of this article can be found under https://doi.org/10.1002/smll.202400784

[+]Present address: School of Mechanical Engineering and State Key Laboratory of Mechanical System and Vibration, Shanghai Jiao Tong University, Shanghai 200240, China

© 2024 The Authors. Small published by Wiley-VCH GmbH. This is an open access article under the terms of the Creative Commons Attribution License, which permits use, distribution and reproduction in any medium, provided the original work is properly cited.

DOI: 10.1002/smll.202400784

K. Sun Michigan Center for Materials Characterization University of Michigan

Ann Arbor, MI 48109, USA A. Tuteia

Department of Chemical Engineering University of Michigan Ann Arbor, MI 48109, USA

A. Tuteja
Department of Macromolecular Science and Engineering
University of Michigan
Ann Arbor, MI 48109, USA

A. Tuteja BioInterface Institute University of Michigan Ann Arbor, MI 48109, USA

www.small-journal.com

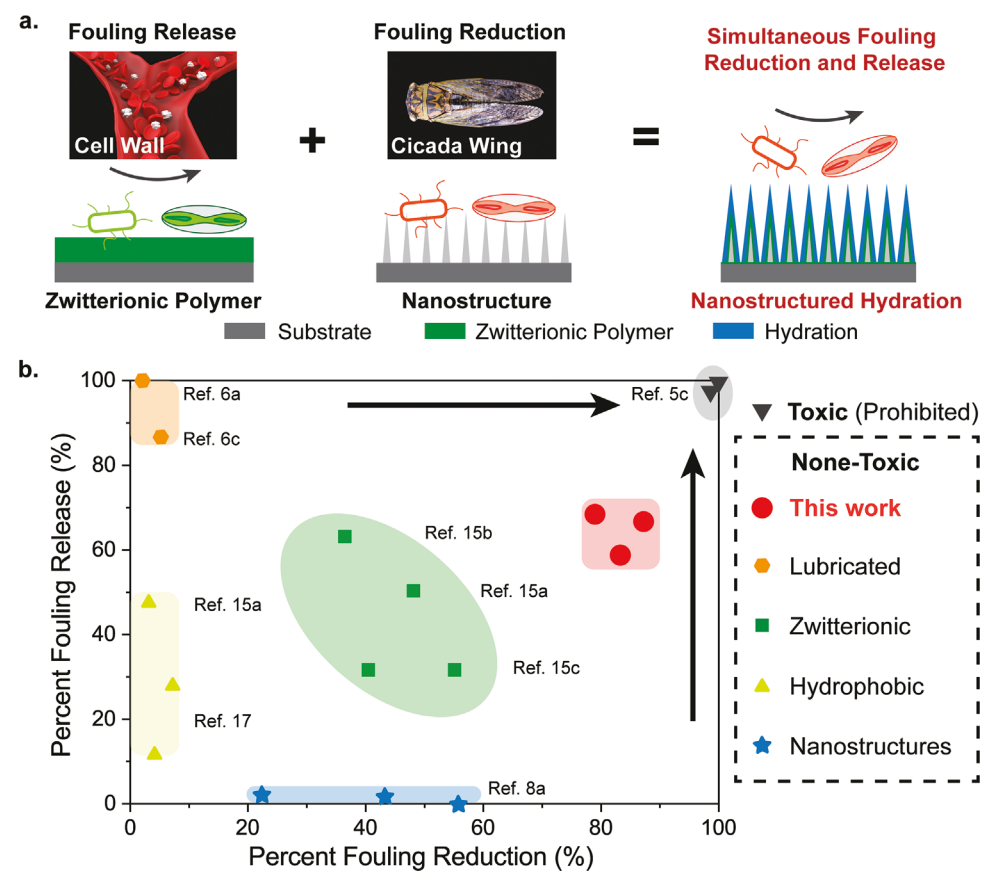


Figure 1. Bioinspired zwitterionic nanowire coatings that are capable of simultaneous fouling reduction and fouling release. a) Schematics of the bioinspired antifouling strategies employed in thus study. b) Comparison of various state-of-the-art antifouling coatings with respect to fouling reduction and fouling release performance. The control samples studied in this work include oil-infused slippery surfaces, zwitterionic polymer coatings, hydrophobic polydimethylsiloxane (PDMS) coatings, [21] and functionalized ZnO nanowire structures. Toxic marine paints, which are prohibited, are also included in this chart. ZNWs demonstrate the highest simultaneous levels of fouling reduction and release.

The current design strategies for marine coatings aim toward either fouling reduction or fouling release. [1b] Fouling reduction attempts to significantly delay the biofilm growth, while fouling release results in the easier removal of accumulated biofilms. Over the past century, only highly toxic marine paints have proven to be effective in simultaneously reducing and releasing marine fouling.<sup>[5]</sup> After a ban was placed on these paints in 2008 because of their environmental issues, [5b,c] a variety of non-toxic marine coatings have been developed in the past decade. These non-toxic coatings have mainly applied two strategies to achieve antifouling performance: 1) creating a physical barrier for attachment (for example, by forming a lubricant layer), [6] and 2) killing marine microbes through the use of either naturally biocidal chemicals<sup>[7]</sup> or via the mechanical biocidal effect, which is inspired by cicada wing surfaces.<sup>[8]</sup> However, to date, these strategies have not achieved effective simultaneous fouling reduction and release behavior that is comparable to the prohibited toxic

Current coatings that employ physical barriers or mild biocides have suffered from significant limitations when they are used for marine antifouling. For example, a physical barrier composed of air generally exists on superhydrophobic surfaces that are inspired by the *Lotus* leaf, which can effectively prevent fouling for a short period of time (e.g., 1–10 days).<sup>[8a,9]</sup> However, once the water breaks through the quasi-stable air layer, fouling species can freely settle and strongly adhere to the surface. As a result of this strong adhesion after water breakthrough, superhydrophobic surfaces typically only reduce fouling and do not promote fouling release. Another recently developed strategy involves the use of liquids (oils or water) as a physical barrier.<sup>[6]</sup> Inspired by the *Nepenthes* pitcher plant rim,<sup>[10]</sup> lubricant-infused surfaces with an oil layer on the surface have demonstrated significant fouling release performance because of their poor adhesion to biofilms,<sup>[6]</sup> but they cannot prevent a variety of fouling species from settling and accumulating on the surface (**Figure 1**). They also lose their lubrication layer easily under applied shear stress.<sup>[11]</sup>

Another physical barrier, which is inspired by blood vessel cell walls, is the stable layer of interfacial water<sup>[12]</sup> that is formed on the surfaces of hydrophilic polymers, for example, polyethylene glycol, zwitterionic, and other hydrophilic polymers.<sup>[13]</sup> In particular, zwitterionic polymers can form hydration layers in salt water and have been reported to exhibit more efficient antifouling performance than polyethylene glycol and other hydrophilic polymer modified surfaces.<sup>[14]</sup> This hydration layer has been particularly effective in preventing protein adsorption,<sup>[15]</sup> a problematic





www.small-journal.com

early-stage fouling species.<sup>[1]</sup> In contrast to surfaces with an interfacial oil layer, surfaces with a hydration layer have demonstrated mild effectiveness in both fouling reduction and release (Figure 1).<sup>[16]</sup>

In addition to these physical and chemical barrier layers, another strategy that has been shown to prevent or reduce fouling is the mechanical biocidal effect. This effect kills microbes by mechanically damaging their cell membranes.<sup>[17]</sup> In our recent work,<sup>[8a]</sup> we demonstrated the ability to limit the attachment and accelerate the death of complex marine algae foulants using hydrothermally grown ZnO nanowire arrays with tunable geometries; however, these mechanical biocidal properties alone were not able to simultaneously achieve a high fouling release performance.<sup>[8a]</sup> In addition to these passive anti-fouling and fouling-release strategies, recent studies<sup>[18]</sup> have developed an active fouling-release method through sweeping micrometer or millimeter scale structures. These structures generate turbulent flow and remove the accumulated biofilms.

Herein, we report a bioinspired zwitterionic nanowire (ZNW) surface layer (Figure 1a) that employs two synergistic antifouling strategies: 1) incorporation of an interfacial hydration layer as a result of the zwitterionic chemistry, and 2) a mechanical biocidal effect from the nanostructure geometry. These ZNW surfaces form a nanostructured hydration layer that enables simultaneous fouling reduction and fouling release, outperforming the state-of-the-art non-toxic marine coatings (Figure 1b).

ZNWs were fabricated using a hydrothermal synthesis process that was seeded by atomic layer deposition (ALD) films. The NW growth was followed by surface-initiated atom transfer radical polymerization (si-ATRP), which resulted in the formation of core-shell nanostructures with precise dimensional control at the nanometer scale. The fabricated ZNWs exhibited underwater superoleophobicity and under-oil superhydrophilicity, which indicates the formation of a hydration layer. [19]

We tested the ZNWs together with various control surfaces in a marine algae fouling environment, and performed foulingrelease tests under low levels of shear flow. The ZNW surfaces exhibited a 70% reduction in the rate of fouling in a static marine environment compared to uncoated planar control surfaces, which is a >25% improvement over our previously report of ZnO NW coatings without a zwitterionic polymer layer.[8a] In addition, the ZNWs achieved 60% fouling release under an applied shear flow that is at least four orders of magnitude lower than the shear stress applied during regular water jet cleaning.<sup>[20]</sup> This low shear stress can be realized at a cruising speed in a marine vessel, which enables the self-removal of accumulated biofilms on ZNW surfaces. The self-cleaning properties of the ZNW array can enable less frequent cleaning and longer usage time of ship hulls. We explored the synergistic antifouling and fouling-release mechanisms of these coatings with a combination of microscopic imaging and a theoretical adhesion analysis. These newly developed ZNW coatings, which include a nanostructured hydration layer, will inspire new applications in maritime applications, deep ocean exploration, and the biomedical industry. Furthermore, the synergetic design method described herein provides a new design framework for non-toxic antifouling coatings.

# 2. Fabrication of Zwitterionic Nanowires and Their Mechanical Durability

The nanowire (NW) arrays used in this study were fabricated using a hydrothermal synthesis process that was seeded by ALD seed layers (**Figure 2a**), as reported in our previous works. [8a,22] The use of ALD seed layers allows for tunable inter-NW spacing, NW diameter, and angular orientation of the NWs relative to the substrate surface. [8a,22] In this study, high-density ZnO NW arrays were fabricated with a diameter of  $\approx\!50$  nm, inter-NW distance of  $\approx\!40$  nm, and NW length of  $\approx\!800$  nm (Figure S1, Supporting Information). Because the bare ZnO nanowires were observed to be relatively unstable in a saline solution, they were conformally coated with a protective layer of 10-nm Al<sub>2</sub>O<sub>3</sub> by ALD to form a ZnO@Al<sub>2</sub>O<sub>3</sub> core-shell NW geometry. [8a]

It has been previously demonstrated that zwitterionic polymers can be grafted onto the surface of silica-based materials through surface-initiated atom transfer radical polymerization (si-ATRP) process.<sup>[23]</sup> This si-ATRP process usually requires the use of an acid or base catalyst to effectively graft the initiator molecules onto the substrate.[23] In our initial attempts to apply an acid-catalyzed process to the ZnO@Al2O3 core-shell NWs, we observed that the inner ZnO core was etched, resulting in the formation of hollow Al<sub>2</sub>O<sub>3</sub> nanotubes (Figure S2, Supporting Information). To overcome this chemical instability, we modified the surface initiation reaction by utilizing a small amount of water under mild heating conditions as the catalyst to hydrolyze the initiator silane, prior to the subsequent polysulfobetaine methacrylate (pSBMA) ATRP polymerization. This modified polymer grafting method successfully avoids the partial dissolution of the underlying ZnO/Al<sub>2</sub>O<sub>2</sub> NW template, and the zwitterionic polymerization yields a conformal pSBMA brush layer onto the ZnO/Al<sub>2</sub>O<sub>3</sub> core-shell NW surface (Figure 2b,c).

One advantage of this synthesis procedure is the ability to precisely control the growth of core-shell NWs with tunable geometric parameters on a variety of substrates, including convex and concave surface topologies, polymers, fibers, and even biological templates.  $^{\text{[22b]}}$  The areal coverage of the ZNW coating can be easily scaled from 10 to >100  $\text{mm}^2$  and applied to various substrates. Therefore, the synthesis approach introduced here for ZNWs has the potential to form antifouling surfaces on a wide range of surfaces for various end-use applications.

The fabricated ZNWs can withstand high fluid shear (70 MPa) under 20 kHz sonication<sup>[24]</sup> for 10 min (Figure S3, Supporting Information). We also performed a harsh Taber mechanical abrasion test on the ZNWs (Figure S4a, Supporting Information and Experimental Section), and found that the ZNWs were mostly fractured at the middle of their length, rather than being completely detached from the surface (Figure S4b, Supporting Information). These durability results indicate that ZNWs are mechanically durable under high-pressure fluid environments and can partially withstand harsh mechanical abrasion conditions. In addition, the ZNW surface architectures grown on glass slides were highly transparent (Figure S5, Supporting Information), which can enable marine applications that requiring high optical transmittance, such as underwater sensors and windows. In contrast, we note that all commercial anti-fouling paints are optically opaque.

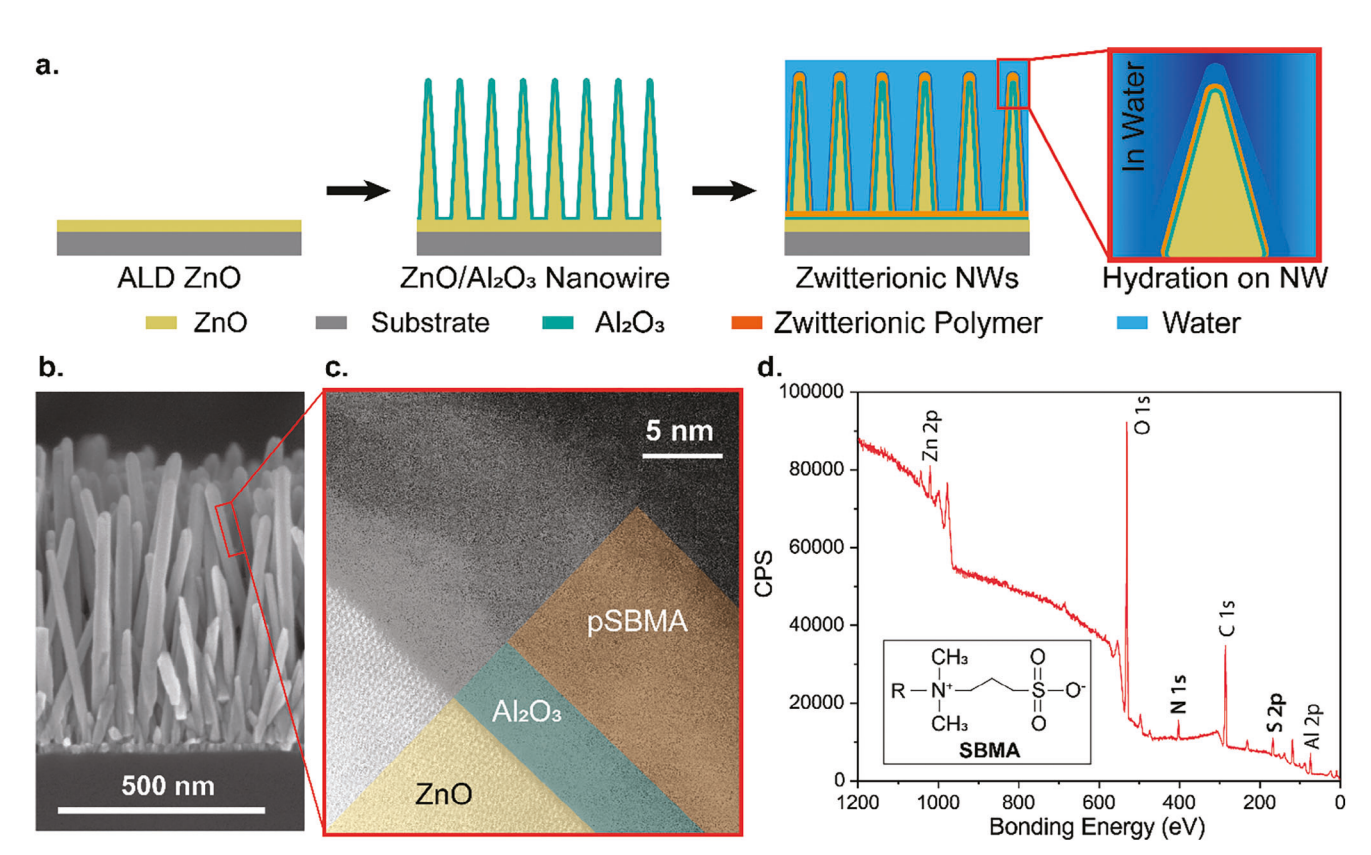


Figure 2. Fabrication and chemical characterization of ZNWs. a) Schematic of the fabrication process and the formation of a hydration layer on ZNWs that are submerged in water. b) SEM image of a ZNW array after polymer grafting, showing that the underlying NW template geometry is maintained. c) STEM image of a ZNW, demonstrating the core-shell-shell architecture. d) XPS spectrum of a ZNW array grown on a silicon substrate, and the chemical structure of SBMA.

## 3. Materials Characterization of the Zwitterionic Nanowires

#### 3.1. Chemical Characterization

To confirm that the geometry of the underlying NW template remained intact after fabrication of the ZnO/Al $_2$ O $_3$ /zwitterionic polymer core-shell-shell architecture, cross-sectional scanning electron microscope (SEM) analysis was performed. As shown in Figure 2b, the resulting ZNWs were closely packed with an aspect ratio of  $\approx\!16$ . This high-aspect ratio nanostructured geometry enables the ZNWs to puncture through cell membrane and mechanically cause death of the bacteria, which is in agreement with model predictions that mechanical biocide can occur in nanostructures with an aspect ratio  $>\!10$ .  $^{[25]}$ 

The ZNWs were analyzed by scanning transmission electron microscopy (STEM) with elemental mapping (Figure 2c; Figure S6, Supporting Information). The STEM image in Figure 2c clearly shows the core-shell-shell structure of the nanowires with a single-crystalline ZnO core, an amorphous ALD Al<sub>2</sub>O<sub>3</sub> inner shell, and a pSBMA outer shell. Elemental maps of Zn, Al, and S also confirmed the distinct chemical composition of these three layers (Figure S6, Supporting Information). In particular, the geometry is confirmed by the localization of the Zn, Al, and S signals in the core ZnO NW, Al<sub>2</sub>O<sub>3</sub> inner shell, and pSBMA outer shell regions, respec-

tively (Figure S6b, Supporting Information). Additional STEM-EDS element mapping is provided in Figure S7 (Supporting Information).

X-ray photoelectron spectroscopy (XPS) analysis was also performed to characterize the surface chemistry of the ZNWs, to confirm the chemical composition of the outer zwitterionic polymer shell. The XPS spectrum exhibited the presence of all the constituent elements (Zn, Al, S, C, and N) in the zwitterionic NWs. As expected for pSBMA, the ratio of the atomic percentage of sulfur to nitrogen was  $\approx 1\text{-to-}1$  (Table S1, Supporting Information). Collectively, these data provide evidence of the successful grafting of pSBMA onto the underlying ZnO/Al $_2$ O $_3$  core-shell NW template.

### 3.2. Wetting Characterization

Zwitterionic polymers are known for their high affinity to water molecules because they incorporate both positive and negative charges in their structures.<sup>[26]</sup> Water molecules are strongly attracted to the charged functional groups and form a thermodynamically stable water layer, resulting in the repellency of various proteins from the polymer surface.<sup>[15a]</sup> This water layer also serves as a lubricating layer, which blocks not only other immiscible liquids such as oils, but also larger biofouling species that may come into contact with the solid zwitterionic polymer.<sup>[23a]</sup>

SMQ

www.small-journal.com

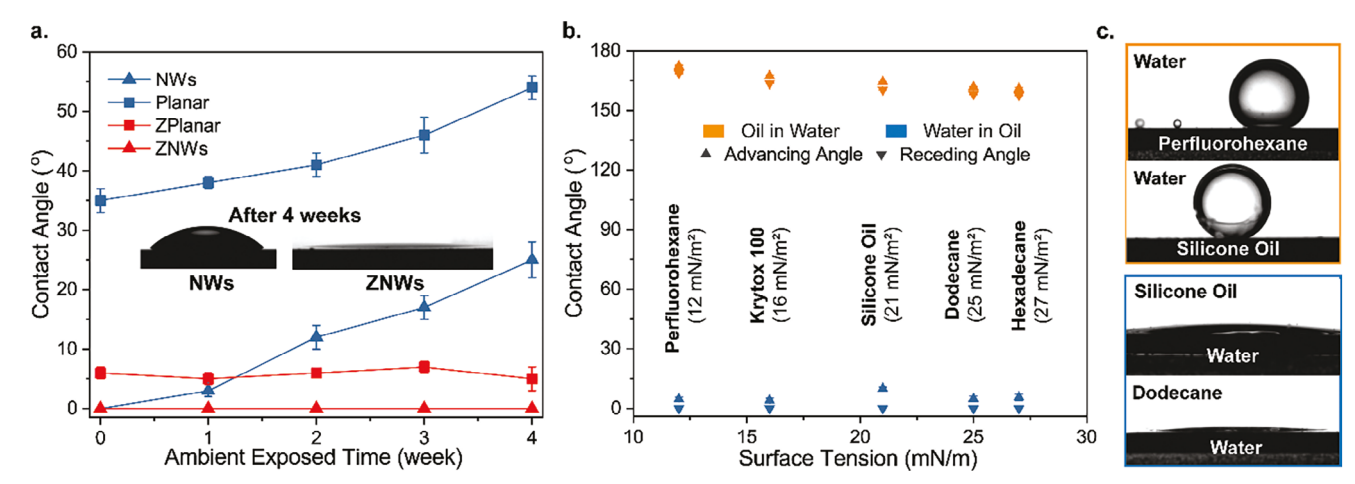


Figure 3. Contact angle measurements on ZNWs and uncoated NWs using different combinations of water and oils as the bath and droplet liquids. a) Contact angle measurement of water droplets on different surfaces after various exposure times to oil vapor. The inset photos present water droplets on NWs and ZNWs after 4 weeks exposing to air. b) Advancing and receding contact angle measurements underwater using different oils as the droplet (orange data points), and under different oils, using water as the droplet (blue data points). The oils tested included perfluorohexane, Krytox 100, silicone oil with a viscosity of 25 cSt, dodecane, and hexadecane. The error bars were obtained from at least three independent measurements. c) Perfluorohexane and silicone oil drops on ZNWs in water environment and water drops on ZNWs in silicone oil and dodecane environments.

Before the fabricated zwitterionic NWs were submerged in a marine fouling environment for testing, their wetting properties were characterized under three different conditions. First, the ZNWs were tested to determine the stability of their wetting behavior under an oil-vapor environment and were compared to other surfaces, including a zwitterionic planar surface, uncoated NWs (i.e., ZnO/Al<sub>2</sub>O<sub>3</sub>), and a planar Al<sub>2</sub>O<sub>3</sub> surface (not coated by the zwitterionic polymer). A pool of oil was heated to a temperature of 60 °C in close proximity to the testing surfaces, so that the oil vapor could gradually adsorb onto the adjacent surfaces. Subsequently, water contact angle measurements were performed on these surfaces once-per-week for 4 weeks. As shown in Figure 3a, the contact angles of uncoated surfaces with and without NWs increased by ≈20° after 4 weeks. In contrast, the zwitterionic pSBMA coated surfaces with and without NWs did not show any changes in their water contact angle. This is a result of the strong affinity of zwitterionic polymers to water molecules, because macroscopically, water can easily displace the oil contaminant layer on the zwitterionic surfaces.

Second, we measured the underwater contact angles of various oils with different surface tensions on the surfaces of the zwitterionic NWs and uncoated NWs. In these experiments, oil droplets were placed on the testing surfaces in a bath of water. On the zwitterionic NW surfaces, the measured underwater contact angles for the various oils were all above 150°, and the underwater contact angle hysteresis of the oils was consistently below 5° (Figures 3b and 3c; Video S1, Supporting Information). This indicates that the zwitterionic NWs are superoleophobic underwater when they are placed in contact with oils with surface tensions ranging from 12 to 27 mN m $^{-1}$ . In contrast, the oils tested on the uncoated NWs were all in the Wenzel state, with a contact angle hysteresis >25° (Figure S8a, Supporting Information).

Finally, the reverse experiment was performed to measure water contact angles in an oil bath for the zwitterionic NW and uncoated NW samples. None of the surfaces were pre-wetted be-

fore submerging them into separate oil baths. The probing liquid in this case was water, while a variety of oils were used as environmental liquids. As shown in Figures 3b and 3c, the zwitterionic NWs were superhydrophilic when immersed in multiple oils (the water droplet spread onto the ZNW surfaces in the oil bath). In comparison, the uncoated NWs were hydrophobic and were observed to be in the Wenzel state for most of the oils, with the exceptions of dodecane and silicone oil (Figure S8b, Supporting Information). To study the effects of salinity, we tested the wetting behavior of salt water (3.5% sodium chloride) on ZNWs, which demonstrated similar underwater superoleophobicity and underoil superhydrophilicity (see in Table S2, Supporting Information). The results of these underwater and under-oil contact angle measurements further prove that the zwitterionic coated surfaces can form a stable water layer once in contact with water and can repel hydrocarbon-based organic liquids, indicating that the zwitterionic coated NW surfaces possess the ideal wetting properties to prevent the adhesion of hydrocarbon molecules secreted from marine biofoulants.

### 4. Marine Fouling Reduction and Release

In the maritime industry, effectively preventing or reducing fouling in static (non-flow) conditions, as well as efficiently removing fouling under an applied shear force (fluid flow or mechanical scraping), are both desirable. [1a] Therefore, in this section, we present the results of both fouling-reduction and fouling-release experiments on a variety of technologically relevant coatings, including ZNWs, and further reveal the underlying mechanisms that enable the simultaneous fouling reduction and release on ZNW surfaces. In particular, algae mixtures that originally collected from the Atlantic Ocean (Florida, USA), were used in this study as a model marine fouling system, because they are one of the most common and wide-spread biofoulants found in marine fouling environments. [6c,8a]

www.small-journal.com

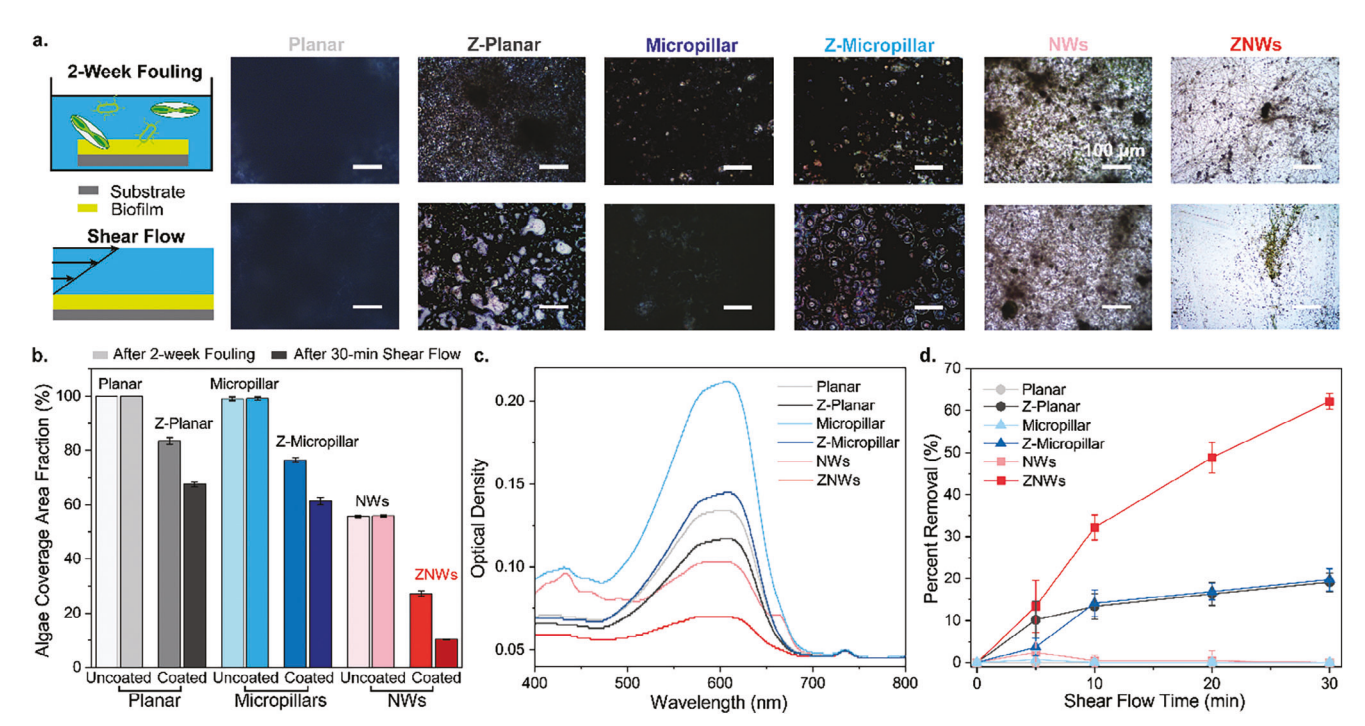


Figure 4. Algae fouling release tests on ZNWs and other coatings. a) Optical microscopy images of the tested surfaces after two weeks of fouling and after 30-min of shear flow. b) Algae coverage area fraction on the tested surfaces after two weeks of fouling and after 30-min of shear flow. c) Optical density measurements of the samples after 30-min of shear flow. d) Percent removal on the tested surfaces as a function of shear flow time. The error bars were obtained from at least three independent measurements.

### 4.1. Marine Fouling Tests on the Zwitterionic Nanowires and Control Surfaces

In the fouling tests, various surface coatings were submerged into a concentrated algae fouling solution and were maintained in a static position for 14 days, after which time 100% of the planar control surface was covered by foulants. The surfaces that were tested included ZNWs, uncoated NWs, zwitterionic planar surfaces, uncoated planar surfaces, zwitterionic micropillars, and uncoated micropillars (further details in the Experimental Section). The micropillars represented surfaces with a sufficiently large feature size that mechanical biocide would be negligible, large feature size that mechanical biocide would be negligible which allowed for an evaluation of the effectiveness in fouling reduction for the smaller-diameter NWs. The fouled surfaces were analyzed using optical microscopy to obtain the fouling area coverage fraction, which is defined as the areal coverage of visible foulants expressed as a percentage of the total sample area measured. [8a]

As shown in the optical microscopy images in Figure 4a, ZNWs exhibited the lowest amount of fouling among all of the surfaces tested, showing significantly less fouling than the planar surfaces, as well as the micropillar samples that were both with and without a zwitterionic polymer coating. Quantitatively, <30% of the surface area of the ZNWs was covered with marine algae (Figure 4b), while 100% of the surface area was covered by algae on uncoated planar and micropillar surfaces. In addition, >75% of the surface area was covered by algae on zwitterionic planar and micropillar surfaces, and 55% of the surface area was covered by algae on uncoated NWs (detailed area coverage fraction values are provided in Table S3, Supporting Information). Over-

all, the ZNWs exhibited >25% improvement in fouling reduction compared to the state-of-the-art anti-fouling nanostructures after 14 days.

### 4.2. Fouling Release on the Zwitterionic Nanowires and Control Surfaces

Fouling release tests were performed using an open-channel flow configuration (Figure S9, Supporting Information) to generate a controllable wall shear to study the removal of the attached biofilms. This open-channel flow setup can generate a shear stress of 0.4 Pa (detailed discussion in the Supporting Information and Table S4, Supporting Information). Thirty minutes of shear flow was applied on the fouled surfaces. Under these mild flow conditions, only the surfaces coated with zwitterionic polymers successfully demonstrated fouling release (Figure 4a,b). Three different characterization methods were applied to quantify the fouling release performance: area coverage, biofilm volume, and biofilm removal rate.

The total area that remained covered by algae after the flow tests was measured using optical microscopy. [8a] In particular, the fouling coverage fraction on the ZNWs dropped from 28% to 10% (Figure 4b), which can be seen in the optical microscopy images (Figure 4a). The zwitterionic-coated planar and micropillar surfaces also displayed a lower extent of algal fouling coverage after 30 min of shear flow; however, their final coverage fractions were still six times higher than ZNWs (Figure 4b).

To quantify the total volume of foulants that remained on the surface, optical density measurements were performed after



www.small-journal.com

30 min of shear flow. The optical density measurement technique is a destructive method used to quantitatively characterize the fouling coverage in a 3D manner. [8a] The optical absorbance of a biological stain is measured with UV-vis spectrometry after removal of the adhered biofilm from the surface, which provides a measurement of the total volume of attached cells on the surface (further details in Experimental Section). From the optical density measurements shown in Figure 4c, the uncoated micropillar surfaces exhibited nearly twice the volume of attached cells compared to that of the uncoated planar surfaces, which could not be fully captured by the 2D optical microscopy measurements. Interestingly, the optical density of the uncoated planar surfaces was only four times larger than the ZNWs after 30 min of shear flow, while their areal coverage fraction was >ten times higher than ZNWs (Figure 4b). This indicates that algae cells tend to grow in a horizontal direction on favorable planar surfaces. In contrast, they tend to grow more vertically on unfavorable surfaces (e.g., ZNWs), because they cannot settle and attach easily onto these substrates.

To quantify the fouling release rate, we also characterized the fouling release performance based on the percentage of algae removal as a function of the time of applied shear flow. The percent removal is defined as the ratio (in percentage) of surface area cleaned by shear flow compared to the surface area that was fouled prior to applying the shear flow. As shown in Figure 4d, the percent removal on the ZNWs continually increased as the shear flow time increased throughout a 30-min shear flow test until it reached >60%. In contrast, the percent removal plateaued at ≈15% after 10 min of shear flow on the zwitterionic coated planar and micropillar surfaces. To contextualize these results, we note that the value of shear stress applied in this study is at least four orders of magnitude lower than the shear stress generated by the high-pressure water jets currently for ship hull cleaning. [23a] It is also lower than the shear stress generated from a typical boat at its cruise speed, [27] indicating that the accumulated marine fouling in static condition could be removed when driving a boat in the marine environment.

### 4.3. Mechanism of Simultaneous Fouling Reduction and Release of ZNWs

Because the ZNWs simultaneously exhibited excellent fouling-reduction and fouling-release performance, an improved understanding of the underlying mechanisms that produce these phenomena would provide novel design principles for future antifouling surfaces. Therefore, in this section, we separately explored the mechanisms of fouling-reduction and fouling-release behavior on ZNWs through experimental observations and interface adhesion models.

First, we examine the mechanism of the fouling-reduction on ZNWs. As we have shown in our previous study, [8a] the fouling reduction on the uncoated NWs was mainly attributed to the mechanical biocidal effects from the high-aspect-ratio NW structures (>95% death rate). [25] Therefore, to explore the biocidal capability of ZNWs, we applied a live/dead stain to the accumulated algal film on uncoated NWs and ZNWs, and found that both uncoated NWs and ZNWs observed a significant biocidal effect ( $\approx$ 97% death rate), as shown in **Figure 5a**—c. Interestingly, the

rate of fouling reduction on ZNWs (>72% relative to uncoated planar control) is >1.6  $\times$  faster than that of the uncoated NWs (45% relative to uncoated planar control) (Figure 4b), although they have similar mechanical biocidal rates. Since the only difference between the uncoated NWs and ZNWs is the surface chemistry, this enhancement in fouling-reduction on ZNWs could be attributed to the zwitterionic polymer layer.

As shown in previous studies, [15a,26b] the physicochemical properties of the zwitterionic polymers result in mild fouling-reduction performance. In particular, zwitterionic polymers can form a hydration layer to reduce the adhesion from the proteins secreted by the marine species. This reduced adhesion also slightly delays the settlement and nucleation of marine species (Figure 4a–c), but it does not cause them to die, as shown by the lack of dead cells accumulated on the surface (Figure 5a,b). In contrast, zwitterionic NWs can form a nanostructured hydration layer that conformally covers the NWs. This nanostructured hydration synergistically leverages both mechanisms: the mechanical biocidal effect from the NW geometry, and the surface chemistry effect of the zwitterionic polymer to achieve enhanced fouling reduction.

Next, we examine the contributions of the ZNW geometry on the fouling release behavior. Through cross-sectional SEM images of biofilms on uncoated NWs and ZNWs (Figure 5d; Figure S10, Supporting Information), the biofilms that formed were observed to be localized on top of the NW structures on both surfaces, rather than conformally penetrating into the inter-NW spacing. As a result, only the tips of the NWs were in contact with the biofilm. This results in a reduction in the substrate-biofilm contact area by a factor of  $\approx 33\%$  compared to the total projected substrate area, since the biofilms do not contact the substrate in the gap regions between the NW tips (see detailed discussion in the Supporting Information and Figure S11, Supporting Information). This reduced contact area can result in a reduction in the total adhesion energy, as the adhesion energy (W) is linearly proportional to contact area and work of adhesion, expressed as:

$$W = w_a \times A \tag{1}$$

where  $w_a$  is the work of adhesion and A is the contact area.

As shown in Figure 4d, uncoated NWs did not exhibit any fouling-release performance, while ZNWs demonstrated significant fouling release. This difference in fouling-release performance indicates that the zwitterionic chemistry is the main contributor to fouling release. On the other hand, zwitterionic planar surfaces and zwitterionic micropillars, which have a larger contact area with the biofilms (Figure 5d), showed less fouling release (Figure 4d) than ZNWs. This phenomenon reveals the importance of reducing contact area to achieve efficient fouling-release. These experimental and theoretical analyses indicate that the NW geometry can effectively reduce the contact area to the biofilms by only contacting the tips of the NWs, and that the zwitterionic surface chemistry can reduce the work of adhesion.

To understand the origins of the observed reduction in contact area between the NWs and the biofilms that are attached on the top surface, we applied the Dahlquist criterion. [28] Marine-fouling biofilms are largely composed of viscoelastic bio-adhesives, which have a wide range of elastic modulii from 1 kPa to 1 GPa. [29]

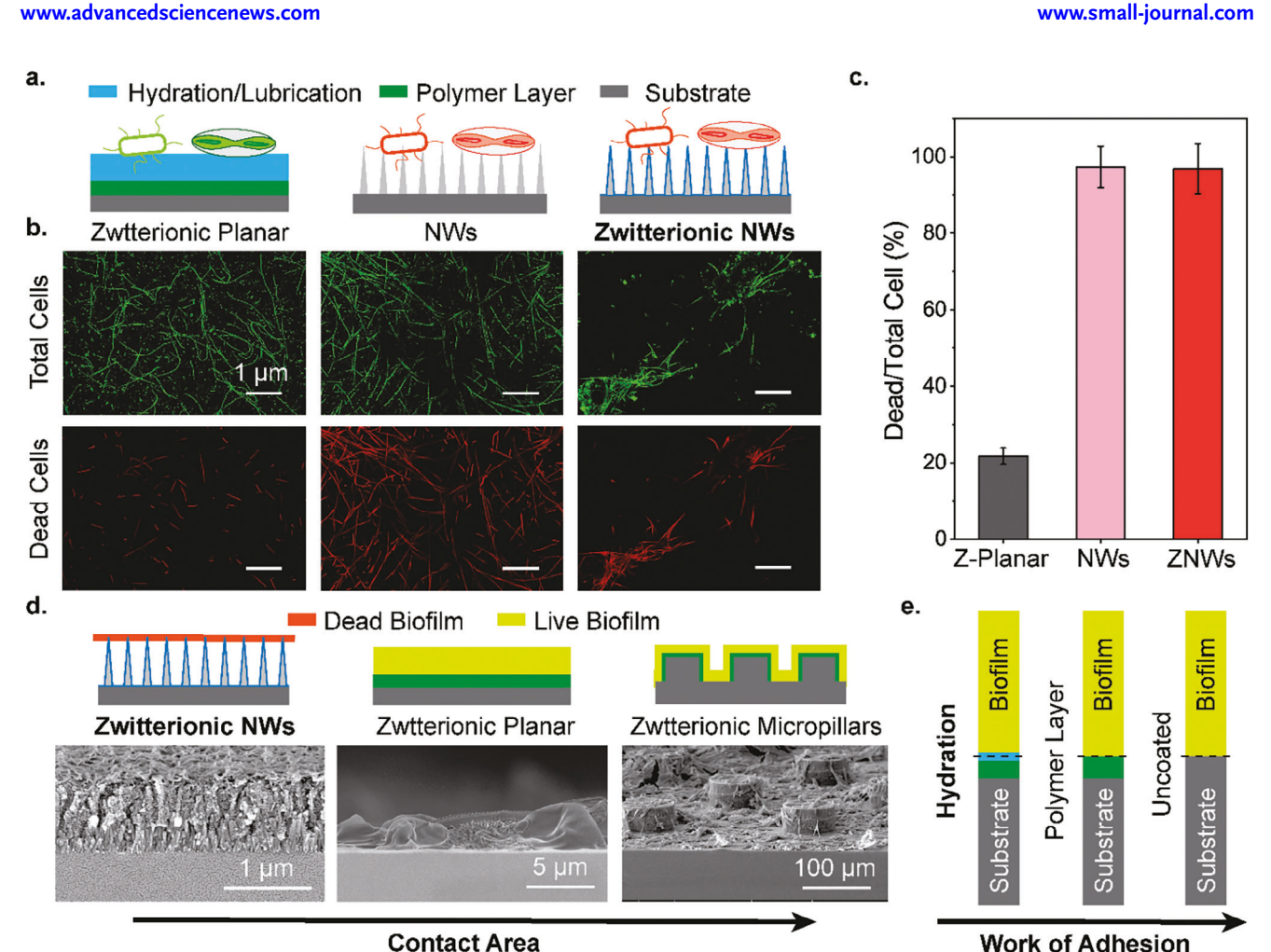


Figure 5. Mechanisms of the simultaneous fouling reduction and fouling release on ZNWs. a) Schematic illustrating the algae activity on hydrated or lubricated surfaces, uncoated NWs, and ZNWs. b) Live/dead cell fluorescent microscopy images of zwitterionic planar, uncoated NW, and ZNW surfaces after 5-day algal fouling. c) Ratio of dead algae cells to total cells on various tested surfaces. d) Cross-sectional SEM images and corresponding schematics showing the contact area of biofilms on different surfaces. e) Schematics illustrating the work of adhesion on different surfaces. The error bars were obtained from at least three independent measurements.

The Dahlquist criterion<sup>[28]</sup> reveals that a viscoelastic adhesive can conformally attach to the surface if its modulus (G) is below a critical modulus value ( $G_c$ ), which is defined as:

$$G_c = W_a \times \sqrt{\frac{R}{h^3}} \tag{2}$$

where  $W_a$  is the work of adhesion, R is the tip radius of the NWs, and h is half of the average height of NWs. In other words, we can reduce the contact area by reducing  $G_c$  so that it is less than *G*, which will result in the viscoelastic biofilm only attaching on the tips of the NW structures. The algae foulants used in this work have a modulus  $\approx 10 \text{ kPa.}^{[29]}$  Based on this information, we found that our NW structure ( $h = 0.8 \mu m$  and R = 25 nm) meets the Dahlquist criterion, [28] for a given work of adhesion  $W_a$  of 100 mJ m<sup>-2</sup> (see detailed discussion in the Supporting Information and Figure \$12, Supporting Information).

To estimate the work of adhesion of the surfaces used in this study, it can be expressed as  $w_a = \gamma_{bl} + \gamma_{sl} - \gamma_{bs}$  for solid-to-solid adhesion,<sup>[30]</sup> where  $\gamma_{bl}$ ,  $\gamma_{sl}$ , and  $\gamma_{bs}$  are the interfacial energy at

the biofilm-to-liquid, surface-to-liquid, and biofilm-to-substrate interfaces, respectively. For a zwitterionic polymer surface with a hydration layer (Figure 5e), the interfacial energy of the hydration layer to liquid (hydration layer-water: 0.4 mJ m<sup>-2</sup>) is significantly lower than that of the underlying inorganic substrate surface-toliquid (Al<sub>2</sub>O<sub>3</sub>-water: 972 mJ m<sup>-2</sup>) (see detailed discussion in the Supporting Information and Table \$5, Supporting Information). This results in a significant decrease in the work of adhesion after polymer grafting, from 16 to 0.8 mJ m<sup>-2</sup>, which improves the resistance of the zwitterionic hydration layer to protein settlement and attachment.[15] In our previous study on superhydrophobic NW arrays that were coated with a low-surface-energy perfluorosilane (16 mJ m<sup>-2</sup>), the silanized surface still has a relatively higher work of adhesion (18 mJ m<sup>-2</sup>) with the algal biofilms (Figure 5e; Table S5, Supporting Information) compared to the ZNW surface. This illustrates the advantage of using a hydration layer to replace the solid-to-solid interface with a liquid-to-solid interface, to promote improved fouling release.

Combining the effects of a low contact area and low work of adhesion, the ZNWs are estimated to have 60 times lower total





www.small-journal.com

adhesion energy than uncoated planar surfaces toward algae biofilms, based on a  $3\times$  reduction in the contact area, combined with a  $20\times$  reduction in the work of adhesion. In addition, we note that the hydration layer provides a  $6\times$  larger contribution to the observed reduction in adhesion energy (i.e., fouling release) than the contact area reduction using ZNWs in this work.

### 5. Conclusion

In summary, inspired by the complimentary antifouling strategies found in different species in nature, we introduced a transparent zwitterionic nanowire coating that is superoleophobic underwater, and simultaneously displays outstanding marine fouling reduction and release. The zwitterionic nanowire coating in aqueous environment is composed a ZnO nanowire core and three concentric shell layers, from the inside to outside: 1) an Al<sub>2</sub>O<sub>3</sub> protection layer; 2) a zwitterionic polymer layer; and 3) a hydration layer formed on the surface of the zwitterionic polymers. The presence of the nanostructured hydration layer enabled the zwitterionic nanowire coatings to achieve a >75% reduction in the rate of algae fouling compared to uncoated planar surfaces. The ZNWs further enabled >60% of the remaining foulants to be easily released under a low wall shear stress, which is four orders of magnitude lower than the levels of water jet flow used in commercial ship hull cleaning. The mechanism of this simultaneous fouling reduction and release is attributed to the synergistic effects of mechanical biocide and the poor adhesion of biofilms to the nanostructured hydration layer. In the future, these ZNW coatings have significant potential applications in the maritime industry, deep ocean exploration, and biomedical industry. Furthermore, the mechanistic insights provided by this work on the simultaneous fouling reduction and fouling release behavior of ZNWs will provide critical insights for the design of future antifouling marine coatings.

### 6. Experimental Section

Materials and Fabrication: Core-shell ZnO@Al2O2 NW arrays were fabricated following previous reports. [8a,22a] First, a 20 nm seed layer of ZnO was coated on the substrate using ALD, followed by 60 min of hydrothermal synthesis of ZnO nanowires. This resulted in nanowires with a length of  $\approx 1~\mu m$ . The ZnO nanowires were subsequently coated with 10 nm of Al<sub>2</sub>O<sub>3</sub> by ALD, to form the chemically protective inner shell. This NW fabrication process can be scaled up by a manufacturing platform for larger macroscopic and non-planar objects, using a flow-reactor that improves process throughput and reduces chemical waste.[31] Before zwitterionic polymer grafting, the NW substrates were treated with a 50 W oxygen plasma (Plasm Etch Inc.) for 20 min to remove any organic contaminent. The plasma treated substrates were submerged into a 8 mg mL<sup>-1</sup> [(3-trimethoxysilyl)propyl 2-bromo-2-methylpropionate] (Gelest) in 1% H<sub>2</sub>O/Ethanol (Sigma-Aldrich) solution. The solution and substrate were then heated on a hotplate at 85 °C for 2 days, followed by heating at 110 °C for 12 h. Once complete, the samples were rinsed with 2-propanol (Sigma-Aldrich) and gently blown dry with nitrogen.

The pSBMA-ATRP solution was prepared following previous work;<sup>[32]</sup> 3.75 g of [2-(Methacryloyloxy)ethyl]dimethyl-(3-sulfopropyl)ammonium hydroxide (SBMA) was purchased from Sigma–Aldrich, and was dissolved in a mixture of 6.75 mL deionized water and 18.25 mL of Methanol (Fischer). The solution was mixed in a two-neck 100 mL round-bottom flask under nitrogen bubbling for 3 h. 166.25 mg of 2,2′-Bipyridyl (Sigma–Aldrich) was mixed into the solution for 30 min, then 76.25 mg of CuBr and

30~mg of  $CuBr_2$  were added and mixed for an additional 30~min under constant nitrogen bubbling and stirring. The solution turned from transparent to a dark red/brown after copper catalyst was added. With the surface-initiated substrates placed at the bottom of a 50~mL glass septa-jar (Fischer), the ATRP solution was quickly poured into the jar and the cap was closed. Nitrogen was then bubbled for the duration of the reaction. Once the reaction was finished (1 h), the samples were removed and rinsed with DI water, followed by sonication in DI water until all residual polymer was removed.

The uncoated micropillars samples were fabricated using photolithography and reactive ion etching, resulting in pillars with a diameter of  $80\,\mu m$ , a height of  $50\,\mu m$ , and pillar-to-pillar spacing of  $100\,\mu m$ . This was followed by a 10 nm overcoat of ALD Al $_2O_3$  to form a consistent surface composition to the ALD-coated NWs. The zwitterionic micropillars were fabricated using a similar zwitterionic polymer grafting process as described above fort the ZNWs.

*Mechanical Abrasion*: The Taber abrasion test was performed using 5750 linear abrasion. A maximum abrasion speed of 60 cycles min<sup>-1</sup> with a travel distance of 100 mm per cycle was applied using a CS-10 abrader and a loading weight of 350 grams.

TEM Imaging: A Thermo-Fisher Talos F200 was used for imaging and elemental mapping. The microscope was operated in scanning transmission electron microscopy (STEM) mode, and the Velos software was used for collecting STEM images including high-angle annular dark-field imaging (HAADF), low angle annular dark field (LAADF) and bright-field (BF) images, and energy-dispersive X-ray spectroscopy (EDS) element maps. Three different zwitterionic NW coatings were analyzed.

Contact Angle Measurements: The underwater and underoil contact angle measurements were performed with a Ramé-Hart 200-F1 contact angle goniometer using the sessile drop method. Advancing and receding contact angles were obtained by measuring the angle while the liquid was slowly added to or removed by a micro-syringe from a  $\approx\!5~\mu L$  droplet in contact with the surface.

Algae Fouling Experiments: Algae mixtures containing multiple species of diatoms and cyanobacteria were used as the fouling species. The algal fouling tests were performed in a manner similar to the previous reports. [6c,8a] Specifically, 2 grams of biomass (i.e., algae biofilm) was weighed using an analytical balance with a resolution of 0.0001 g and was introduced to a petri dish (diameter: 100 mm) with 50 mL of seawater and a F/2 (purchased from https://www.amazon.com/) mixture. Samples were submerged into the algae culture environment for 14 days. Optical microscopy images were taken on these fouled surfaces using a Nikon LV150N Optical Microscope. The algae coverage area fraction was quantified with obtained microscopic images through ImageJ analysis.

Optical Density Measurements: The fouled surfaces were first rinsed by saltwater (0.8 m NaCl) to remove unattached algae, followed by soaking in dimethyl sulfoxide (DMSO) (Sigma–Aldrich, Inc.) for 15 min to remove the chlorophyll in the algae. Then the samples were gently rinsed by saltwater again and stained with trypan blue (from Thermo Fisher Scientific) for 15 min. Next the excess dye was rinsed off using a saline solution. Finally, 10 mL of DMSO was used for each sample to extract the blue stain, and absorbance of the liquid was measured with UV–vis spectrometry.

Live/Dead Cell Microscopic Fluorescent Imaging: The coatings were all submerged in the algal culture solution for 5 days, followed by cleaning in sodium chloride (NaCl) solution (0.85%) with gentle stirring for 15 min. A LIVE/DEAD BacLight Bacterial Viabilty Kit (Thermo Fisher Scientific L7012) was used to stain the fouled samples. The fouled coatings were all stained with the dye solution for 15 min in dark environment. Fluorescent microscope images of each sample were taken using a Nikon A1RSi confocal laser scanning microscope fitted with a Plan Apo Lambda 20x objective. The SYTO 9 and propidium iodide were excited using Coherent OBIS LX/LS 488 nm and Coherent Sapphire 561 nm lasers, respectively. The emissions were collected using the FITC (490–525 nm) and Texas Red (570–620 nm) filters, respectively.

Statistical Analysis: At least three independent measurements were taken for each statistical analysis.



### **Supporting Information**

Supporting Information is available from the Wiley Online Library or from the author.

### **Acknowledgements**

This work was supported by the DARPA Young Faculty Award D18AP00066. Any opinions, findings, conclusions or recommendations expressed in this publication are those of the authors and do not necessarily reflect the views of DARPA. This material is based upon work supported by the National Science Foundation under grant no. 1751590. The authors also thank Dr. Paul Armistead, Dr. Kathy Wahl, and the Office of Naval Research (ONR) for financial support under grant N00014-20-1-2817. The authors thank Dr. Eric Kazyak, and Dr. Julia D. Lenef from University of Michigan for the help of TEM imaging, Dr. Adrian J. Sanchez for the help of micro-structured control surfaces, Dr. Lin Wang from Pennsylvania State University for the cicada photo, and Yixin Chen from Shanghai Jiao Tong University for preparing the blood vessel image.

### **Conflict of Interest**

The authors declare no conflict of interest.

### **Data Availability Statement**

The data that support the findings of this study are available from the corresponding author upon reasonable request.

#### **Keywords**

bioinspiration, marine fouling, nanowires, superoleophobic, zwitterionic

Received: January 30, 2024 Revised: May 10, 2024 Published online:

- a) J. A. Callow, M. E. Callow, Nat. Commun. 2011, 2, 244; b) H. Jin, L.
   Tian, W. Bing, J. Zhao, L. Ren, Prog. Mater. Sci. 2022, 124, 100889.
- [2] X.-T. Wang, H. Liu, Z.-F. Lv, F.-Y. Deng, H.-L. Xu, L.-J. Qi, M.-S. Shi, J.-C. Zhao, S.-X. Zheng, H.-Y. Man, K.-B. He, *Nat. Clim. Change* 2021, 11, 945.
- [3] a) N. V. Gohad, N. Aldred, C. M. Hartshorn, Y. J. Lee, M. T. Cicerone, B. Orihuela, A. S. Clare, D. Rittschof, A. S. Mount, *Nat. Commun.* 2014, 5, 4414; b) M. Schultz, J. Walker, C. Steppe, K. Flack, *Biofouling* 2015, 31, 759.
- [4] B. Gaylord, J. Hodin, M. C. Ferner, Proc. Natl. Acad. Sci. USA 2013, 110, 6901.
- [5] a) I. Omae, Chem. Rev. 2003, 103, 3431; b) K. V. Thomas, S. Brooks, Biofouling 2010, 26, 73; c) K. A. Dafforn, J. A. Lewis, E. L. Johnston, Mar. Pollut. Bull. 2011, 62, 453.
- [6] a) A. B. Tesler, P. Kim, S. Kolle, C. Howell, O. Ahanotu, J. Aizenberg, Nat. Commun. 2015, 6, 8649; b) S. Amini, S. Kolle, L. Petrone, O. Ahanotu, S. Sunny, C. N. Sutanto, S. Hoon, L. Cohen, J. C. Weaver, J. Aizenberg, N. Vogel, A. Miserez, Science 2017, 357, 668; c) J. Wang, B. Wu, A. Dhyani, T. Repetto, A. J. Gayle, T. H. Cho, N. P. Dasgupta, A. Tuteja, ACS Appl. Mater. Interfaces 2022, 14, 22466.
- [7] a) A. Kumar, S. Mills, K. Bazaka, N. Bajema, I. Atkinson, M. V. Jacob, Surf. Coat. Technol. 2018, 349, 426; b) H. Qiu, K. Feng, A. Gapeeva, K. Meurisch, S. Kaps, X. Li, L. Yu, Y. K. Mishra, R. Adelung, M. Baum, Prog. Polym. Sci. 2022, 127, 101516.

- [8] a) J. Wang, S. Lee, A. R. Bielinski, K. A. Meyer, A. Dhyani, A. M. Ortiz-Ortiz, A. Tuteja, N. P. Dasgupta, Adv. Mater. Interfaces 2020, 7, 2000672; b) E. P. Ivanova, J. Hasan, H. K. Webb, V. K. Truong, G. S. Watson, J. A. Watson, V. A. Baulin, S. Pogodin, J. Y. Wang, M. J. Tobin, C. Löbbe, R. J. Crawford, Small 2012, 8, 2489.
- [9] G. B. Hwang, K. Page, A. Patir, S. P. Nair, E. Allan, I. P. Parkin, ACS Nano 2018, 12, 6050.
- a) H. F. Bohn, W. Federle, *Proc. Natl. Acad. Sci. USA* 2004, 101, 14138;
   b) T.-S. Wong, S. H. Kang, S. K. Y. Tang, E. J. Smythe, B. D. Hatton, A. Grinthal, J. Aizenberg, *Nature* 2011, 477, 443.
- [11] J. S. Wexler, I. Jacobi, H. A. Stone, Phys. Rev. Lett. 2015, 114, 168301.
- a) C. Leng, S. W. Sun, K. X. Zhang, S. Y. Jiang, Z. Chen, Acta Biomater. 2016, 40, 62; b) U. Raviv, J. Klein, Science 2002, 297, 1540; c)
   A. Gaisinskaya, L. Ma, G. Silbert, R. Sorkin, O. Tairy, R. Goldberg, N. Kampf, J. Klein, Faraday Discuss. 2012, 156, 217.
- [13] a) T. Kang, X. Banquy, J. Heo, C. Lim, N. A. Lynd, P. Lundberg, D. X. Oh, H.-K. Lee, Y.-K. Hong, D. S. Hwang, J. H. Waite, J. N. Israelachvili, C. J. Hawker, ACS Nano 2016, 10, 930; b) S. Park, M. Kim, J. Park, W. Choi, J. Hong, D. W. Lee, B.-S. Kim, Biomacromolecules 2021, 22, 5173; c) E. Shin, C. Lim, U. J. Kang, M. Kim, J. Park, D. Kim, W. Choi, J. Hong, C. Baig, D. W. Lee, B.-S. Kim, Macromolecules 2020, 53, 3551; d) L. Li, B. Yan, L. Zhang, Y. Tian, H. Zeng, Chem. Commun. 2015, 51, 15780; e) W. Yang, Z. Zhao, M. Pan, L. Gong, F. Wu, C. Huang, X. Wang, J. Wang, H. Zeng, J. Colloid Interface Sci. 2022, 625, 628.
- [14] a) C.-M. Xing, F.-N. Meng, M. Quan, K. Ding, Y. Dang, Y.-K. Gong, Acta Biomater. 2017, 59, 129; b) J. B. Schlenoff, Langmuir 2014, 30, 9625.
- [15] a) S. Jiang, Z. Cao, Adv. Mater. 2010, 22, 920; b) S. Chen, J. Zheng, L. Li, S. Jiang, J. Am. Chem. Soc. 2005, 127, 14473; c) H. Huang, C. Zhang, R. Crisci, T. Lu, H.-C. Hung, M. S. J. Sajib, P. Sarker, J. Ma, T. Wei, S. Jiang, Z. Chen, J. Am. Chem. Soc. 2021, 143, 16786.
- [16] a) R. B. Bodkhe, S. J. Stafslien, J. Daniels, N. Cilz, A. J. Muelhberg, S. E. M. Thompson, M. E. Callow, J. A. Callow, D. C. Webster, *Prog. Org. Coat.* 2015, 78, 369; b) P. Shivapooja, Q. Yu, B. Orihuela, R. Mays, D. Rittschof, J. Genzer, G. P. López, *ACS Appl. Mater. Interfaces* 2015, 7, 25586; c) M. R. Hibbs, B. A. Hernandez-Sanchez, J. Daniels, S. J. Stafslien, *Biofouling* 2015, 31, 613; d) A. Rahimi, S. J. Stafslien, L. Vanderwal, J. A. Finlay, A. S. Clare, D. C. Webster, *Prog. Org. Coat.* 2020, 149, 105931.
- [17] a) E. P. Ivanova, J. Hasan, H. K. Webb, G. Gervinskas, S. Juodkazis, V. K. Truong, A. H. F. Wu, R. N. Lamb, V. A. Baulin, G. S. Watson, J. A. Watson, D. E. Mainwaring, R. J. Crawford, *Nat. Commun.* 2013, 4, 2838; b) J. Jenkins, J. Mantell, C. Neal, A. Gholinia, P. Verkade, A. H. Nobbs, B. Su, *Nat. Commun.* 2020, 11, 1626.
- [18] a) H. Gu, S. W. Lee, J. Carnicelli, T. Zhang, D. Ren, *Nat. Commun.* 2020, 11, 2211; b) Q. Wu, H. Yan, L. Chen, S. Qi, T. Zhao, L. Jiang, M. Liu, *Adv. Mater.* 2023, 35, 2212246.
- [19] a) C. Leng, H.-C. Hung, S. Sun, D. Wang, Y. Li, S. Jiang, Z. Chen, ACS Appl. Mater. Interfaces 2015, 7, 16881; b) G. Cheng, M. Liao, D. Zhao, J. Zhou, Langmuir 2017, 33, 1732.
- [20] F. Cassé, S. J. Stafslien, J. A. Bahr, J. Daniels, J. A. Finlay, J. A. Callow, M. E. Callow, Biofouling 2007, 23, 121.
- [21] M. J. Vucko, A. J. Poole, C. Carl, B. A. Sexton, F. L. Glenn, S. Whalan, R. de Nys, *Biofouling* **2014**, *30*, 1.
- [22] a) A. R. Bielinski, M. Boban, Y. He, E. Kazyak, D. H. Lee, C. Wang, A. Tuteja, N. P. Dasgupta, ACS Nano 2017, 11, 478; b) A. R. Bielinski, E. Kazyak, C. M. Schlepütz, H. J. Jung, K. N. Wood, N. P. Dasgupta, Chem. Mater. 2015, 27, 4799; c) A. R. Bielinski, A. J. Gayle, S. Lee, N. P. Dasgupta, ACS Appl. Mater. Interfaces 2021, 13, 52063.
- [23] a) Z. Zhang, J. A. Finlay, L. Wang, Y. Gao, J. A. Callow, M. E. Callow, S. Jiang, *Langmuir* 2009, 25, 13516; b) Y. L. Khung, D. Narducci, *Adv. Colloid Interface Sci.* 2015, 226, 166.
- [24] R. Kohli, K. L. Mittal, Developments in Surface Contamination and Cleaning, Elsevier, Amsterdam, Netherlands 2013.

SMQ

www.advancedsciencenews.com

www.small-journal.com

- [25] W. Zhu, A. von dem Bussche, X. Yi, Y. Qiu, Z. Wang, P. Weston, R. H. Hurt, A. B. Kane, H. Gao, *Proc. Natl. Acad. Sci. USA* 2016, 113, 12374.
- [26] a) B. O. Leung, Z. Yang, S. S. Wu, K. C. Chou, Langmuir 2012, 28, 5724; b) Q. Shao, S. Jiang, Adv. Mater. 2015, 27, 15.
- [27] a) P. Esquivel De Pablo, Analysis of the shear stress distributions on two ship hull form, 2014; b) G. K. Choudhary, K. M. Doshi, *Ocean Engineering* 2015, 108, 678.
- [28] a) C. A. Dahlquist, R. L. Patrick in *Treatise on Adhesion and Adhesives*, Vol. 2, Marcel Dekker, New York, USA 1969, p. 219; b) S. Abbott, *The Science of Adhesion*, Royal Society of Chemistry, London, UK 2020.
- [29] a) A. K. Halvey, B. Macdonald, A. Dhyani, A. Tuteja, *Philos. Trans. Royal Soc. A* 2019, *377*, 20180266; b) A. Dhyani, J. Wang, A. K. Halvey, B. Macdonald, G. Mehta, A. Tuteja, *Science* 2021, *373*, eaba5010.
- [30] J. N. Israelachvili, Intermolecular and surface forces, Academic Press, Massachusetts, USA 2011.
- [31] A. M. Ortiz-Ortiz, A. J. Gayle, J. Wang, H. R. Faustyn, D. Penley, C. Sherwood, A. Tuteja, N. P. Dasgupta, ACS Appl. Eng. Mater. 2023, 1, 1583.
- [32] S. Chernyy, M. Järn, K. Shimizu, A. Swerin, S. U. Pedersen, K. Daasbjerg, L. Makkonen, P. Claesson, J. Iruthayaraj, ACS Appl. Mater. Interfaces 2014, 6, 6487.